J. Fluid Mech. (2024), *vol*. 1001, R1, doi:10.1017/jfm.2024.975

The vertical-velocity skewness in the inertial sublayer of turbulent wall flows

Elia Buono[1,2,†], Gabriel Katul[1], Michael Heisel[3], Davide Vettori[2], Davide Poggi[2], Cosimo Peruzzi[4] and Costantino Manes[2]

[1]Department of Civil and Environmental Engineering, Duke University, Durham, NC 27708, USA

[2]Dipartimento di Ingegneria dell'Ambiente, del Territorio e delle Infrastrutture, Politecnico di Torino, 10129 Torino, Italy

[3]School of Civil Engineering, University of Sydney, 2008 Sydney, Australia

[4]Area for Hydrology, Hydrodynamics, Hydromorphology and Freshwater Ecology, Italian Institute for Environmental Protection and Research, 00144 Rome, Italy

(Received 20 July 2024; revised 3 September 2024; accepted 20 September 2024)

Empirical evidence is provided that within the inertial sublayer (i.e. logarithmic region) of adiabatic turbulent flows over smooth walls, the skewness of the vertical-velocity component S_w displays universal behaviour, being a positive constant and constrained within the range $S_w \approx 0.1$–0.16, regardless of flow configuration and Reynolds number. A theoretical model is then proposed to explain this behaviour, including the observed range of variations of S_w. The proposed model clarifies why S_w cannot be predicted from down-gradient closure approximations routinely employed in large-scale meteorological and climate models. The proposed model also offers an alternative and implementable approach for such large-scale models.

Key words: turbulent boundary layers

1. Introduction

Much of the effort devoted to the study of adiabatic and hydrodynamically smooth-wall turbulence has focused on the characterization of velocity statistics within the so-called logarithmic or inertial sublayer (ISL). The attached eddy model (AEM), which is probably the most cited model for ISL turbulence, predicts that first- and second-order velocity statistics can be described as (Townsend 1976; Smits, McKeon & Marusic 2011; Marusic

† Email address for correspondence: elia.buono@polito.it

& Monty 2019):

$$\bar{u}^+ = \frac{1}{\kappa}\log(z^+) + A; \quad \sigma_u^{2+} = A_u - B_u \log\left(\frac{z}{\delta}\right); \tag{1.1a,b}$$

and, a less studied outcome, $\sigma_w^{2+} = A_w^2$, where u and w are the longitudinal and wall-normal velocity components, respectively; z is the wall-normal coordinate; $\sigma_u = \sqrt{\overline{u'^2}}$ and $\sigma_w = \sqrt{\overline{w'^2}}$ are the standard deviation of u and w, respectively; primes identify fluctuations due to turbulence around the mean; the overline represents averaging over coordinates of statistical homogeneity; the plus index indicates classical inner scaling whereby velocities and lengths are normalized with the friction velocity u_* and viscous length scale ν/u_*, respectively, with ν being the kinematic viscosity of the fluid; δ is the outer length scale of the flow; κ, A, A_u, A_w, B_u are coefficients that are thought to attain asymptotic constant values at very large Reynolds numbers $Re_\tau = u_*\delta/\nu$ (Smits *et al.* 2011; Marusic *et al.* 2013; Stevens, Wilczek & Meneveau 2014).

The AEM has been extended to velocity moments of any order as well as cross-correlations between different velocity components thereby providing an expanded picture of ISL flow statistics (Woodcock & Marusic 2015). However, convincing empirical support for the aforementioned theoretical predictions is limited to the statistics of u (Smits *et al.* 2011; Banerjee & Katul 2013; Marusic *et al.* 2013; Meneveau & Marusic 2013; Huang & Katul 2022). In contrast, the statistics of w have been much less reported and investigated, partly because of the technical difficulties associated with accurately measuring w in the near-wall region of laboratory flows at high Re_τ. As a result, theoretical predictions of w-statistics have received mixed support from the literature (Zhao & Smits 2007; Morrill-Winter *et al.* 2015; Örlü *et al.* 2017) and higher-order moments of w' are rarely reported but with few notable exceptions (Flack, Schultz & Connelly 2007; Schultz & Flack 2007; Manes, Poggi & Ridolfi 2011; Heisel *et al.* 2020; Peruzzi *et al.* 2020). We argue that this overlook contributed to hiding a universal property of ISL turbulence, which is herein reported and discussed.

The aim of this paper is to demonstrate that the skewness of w', $S_w = \overline{w'^3}/\sigma_w^3$, is a positive z-independent constant and robust to variations in Re_τ within the ISL. Moreover, a theoretical model that explains this observed behaviour and links S_w to established turbulence constants is proposed, leading to satisfactory predictions. Finally, this paper demonstrates that the asymmetry in the probability density function of w', as quantified by S_w, cannot be accounted for with gradient-diffusion representations routinely employed in meteorological and climate models (Mellor & Yamada 1982). Rectifying this limitation is of significance because S_w is recognized as a key feature of climate and meteorological modelling (Wyngaard 2010) impacting various atmospheric phenomena such as cloud formation (Bogenschutz *et al.* 2012; Huang *et al.* 2020; Li *et al.* 2022) and dispersion processes (Bærentsen & Berkowicz 1984; Luhar & Britter 1989; Wyngaard & Weil 1991; Maurizi & Tampieri 1999). Neglecting S_w affects models by underestimating the impact of the asymmetry between ejective eddy motion ($w' > 0$, $u' < 0$) and sweeping eddy motion ($w' < 0$, $u' > 0$), which is a widely accepted feature of the ISL.

Figure 1 reports the variations of S_w with normalized wall-normal distance (z/δ) using data from direct numerical simulations (DNS) (Sillero, Jiménez & Moser 2013), laboratory experiments pertaining to flat plate turbulent boundary layers (TBLs) (Zimmerman 2019; Heisel *et al.* 2020), uniform (Poggi, Porporato & Ridolfi 2002) and weakly non-uniform open channel flows (Manes *et al.* 2011; Peruzzi *et al.* 2020), pipe flows (Zimmerman 2019) and the atmospheric surface layer (ASL) (Priyadarshana & Klewicki 2004), whereby accurate measurements of w are available. This set of data covers an extensive range of Re_τ

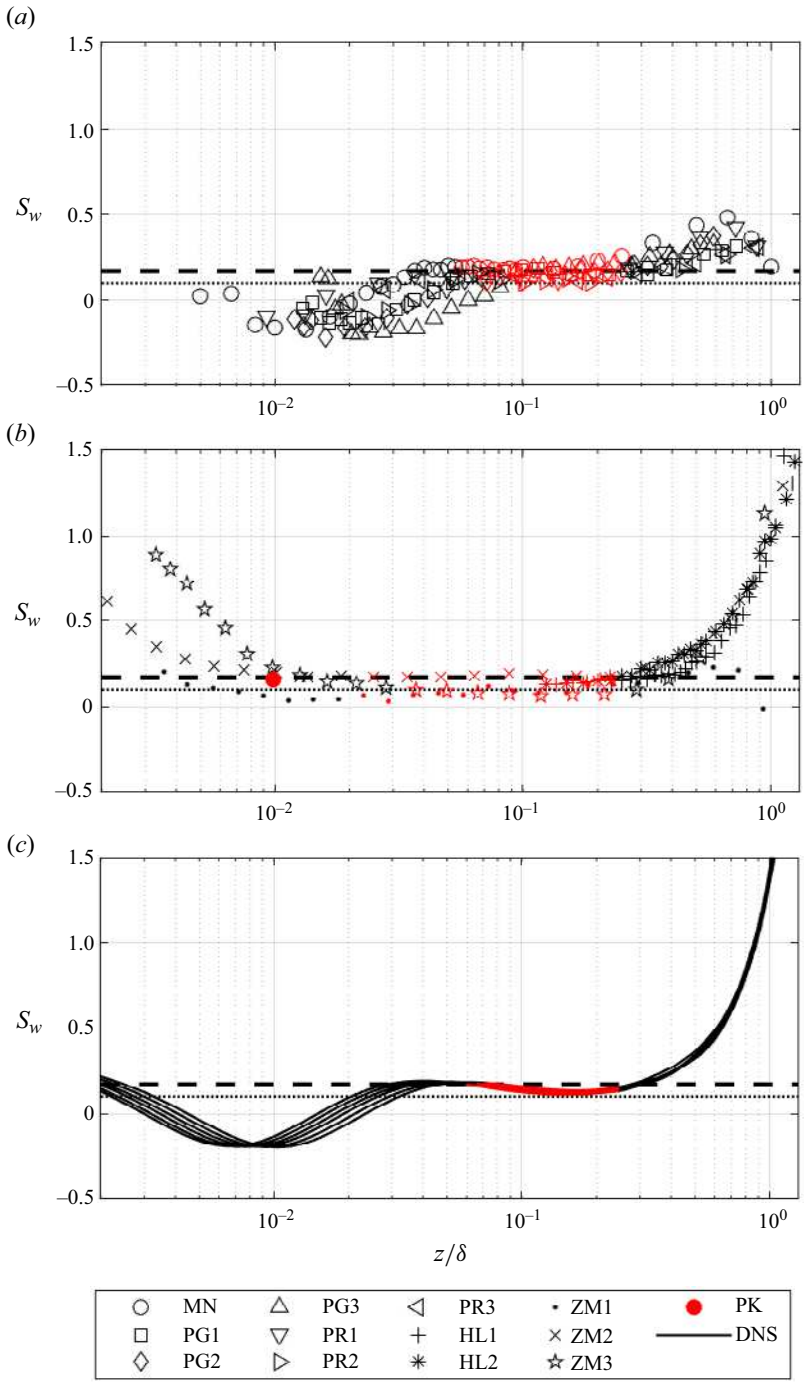

Figure 1. Variation of the vertical-velocity skewness S_w with normalized wall-normal distance z/δ from open channel flow (*a*), wind tunnel, ASL and pipe flow (*b*) and DNS (*c*). The dashed line is $S_w = 0.16$ and the dotted line is $S_w = 0.10$. Data are summarized in table 1. Red symbols and lines identify the ISL range. For HL1 and HL2, near-wall measurements are not reported due to spatial resolution limitations of the x-probe employed in the experiments (Heisel *et al.* 2020).

Source	Data set	Flow	Re_τ	B_u	A_w	S_w
Manes *et al.* (2011)	MN	OC	2160	0.58	1.06	0.11
Sillero *et al.* (2013)	DNS	—	1307	0.85	1.15	0.13
	—	—	÷	—	—	—
	—	—	2000	0.86	1.17	0.12
Heisel *et al.* (2020)	HL1	WT	3800	0.85	0.96	0.21
	HL2	WT	4700	0.63	1.00	0.15
Poggi *et al.* (2002)	PG1	OC	1232	0.73	0.90	0.23
	PG2	OC	1071	0.78	1.02	0.17
	PG3	OC	845	1.03	0.90	0.33
Peruzzi *et al.* (2020)	PR1	OC	2240	0.60	1.12	0.10
	PR2	OC	999	0.48	1.06	0.09
	PR3	OC	1886	0.81	1.06	0.16
Zimmerman (2019)	ZM1	PF	14 005	1.25	1.01	0.28
	ZM2	WT	15 250	1.03	1.26	0.12
	ZM3	WT	6340	0.40	0.81	0.17
Priyadarshana & Klewicki (2004)	PK	ASL	860 000	—	—	—

Table 1. Overview of smooth-wall boundary-layer experiments (OC, open channel/flumes; WT, wind tunnel; PF, pipe flows; ASL, atmospheric surface layer) and DNS (six cases ranging between $Re_\tau = 1307$ and $Re_\tau = 2000$) in figure 1(*c*). The $Re_\tau = \delta u_*/\nu$ is the friction Reynolds number, B_u and A_w were computed from data using AEM. For the DNS, the highest and lowest Re_τ are shown given the small variability in B_u (0.85–0.86) and A_w (1.15–1.17). The computed S_w using (2.11) is also presented.

spanning from 8×10^2 to approx 10^6 (table 1). A reference value of $S_w = 0.1$ is added to the figure as often reported for ASLs in adiabatic conditions across multiple heights and for various surface covers (Chiba 1978). A region of constant S_w weakly varying between 0.1 and 0.16 (here weakly means that variations are much smaller than those displayed by S_w over the entire flow domain) is evident in all profiles within the range $2.6\sqrt{Re_\tau}\nu/u_*$ up to 0.15–0.25δ, which is often associated with the ISL (Zhou & Klewicki 2015; Örlü *et al.* 2016, 2017). This finding is rather remarkable given the large differences in Re_τ, measurement techniques and experimental facilities used. In what follows, a theoretical model that predicts and explains such a behaviour is provided.

2. Theory

To explain the observed behaviour of S_w, a stationary and planar homogeneous incompressible flow in the absence of subsidence is considered for $\overline{w'^3}$. For these conditions, the model can be derived from the Reynolds-averaged Navier–Stokes equations and is given as (Canuto *et al.* 1994; Zeman & Lumley 1976)

$$\frac{\partial \overline{w'^3}}{\partial t} = 0 = \overbrace{3\sigma_w^2 \frac{\partial \sigma_w^2}{\partial z}}^{\textit{Source/sink}} \overbrace{-\frac{\partial \overline{w'w'^3}}{\partial z}}^{\textit{Turbulent transport}} \underbrace{-3\left(\overline{w'w'\frac{\partial p'}{\partial z}}\right)}_{\textit{Pressure-velocity destruction}} \underbrace{-2\nu\left(\overline{3w'\frac{\partial w'}{\partial x_i}\frac{\partial w'}{\partial x_i}}\right)}_{\textit{Viscous destruction}}, \quad (2.1)$$

where t is time, p' is the pressure deviation from the mean or hydrostatic state normalized by a constant fluid density ρ and the repeated index i in the viscous term denotes summation over the spatial coordinates ($[x_1, x_2, x_3] = [x, y, z]$). The first two terms on the right-hand side of (2.1) (i.e. those highlighted by overbraces) arise from inertial effects or convective acceleration, the third and fourth terms (i.e. those highlighted by underbraces) arise due to interactions between $w'w'$ and the forces acting on a fluid element (p' and viscous stresses). A quasi-normal approximation for the fourth moment is used (André *et al.* 1976) so that the flatness factor $F_w = \overline{w'^4}/(\sigma_w)^4 = 3 + a$ and the overall inertial term simplifies to

$$-\frac{\partial \overline{w'^4}}{\partial z} + 3\sigma_w^2 \frac{\partial \sigma_w^2}{\partial z} = -(3 + 2a)\sigma_w^2 \frac{\partial \sigma_w^2}{\partial z}, \tag{2.2}$$

where $a \neq 0$ allows for deviations from Gaussian tails ($a = 0$ recovers a Gaussian flatness factor). Usage of a quasi-Gaussian approximation to close a fourth (and even) moment budget makes no statement on the asymmetry (or odd moments) of the w' probability density function, only that large-scale intermittency is near-Gaussian, a finding well supported in the literature (Meneveau 1991) and many phenomenological approaches (Woodcock & Marusic 2015). Models for the pressure-velocity and viscous destruction terms are now needed to integrate equation (2.1). A return-to-isotropy (or Rotta) model (Rotta 1951) given by

$$-2\overline{w'\frac{\partial p'}{\partial z}} = \frac{C_R}{\tau}\left(\frac{\bar{q}}{3} - \sigma_w^2\right), \tag{2.3}$$

may be used as the basis to derive an expression for the pressure-velocity destruction term in (2.1) where $q = u'u' + v'v' + w'w'$ is twice the instantaneous turbulent kinetic energy (TKE), $\bar{q} = 2K$, K is the averaged TKE, v' is the lateral turbulent velocity, and $C_R = 1.8$ is a well-established constant, the Rotta constant (Bou-Zeid *et al.* 2018). The constant C_R relates the so-called relaxation time $\tau = \bar{q}/\bar{\epsilon}$ to the time it takes for isotropy to be attained at the finest scales, where $\bar{\epsilon}$ is the mean TKE dissipation rate. Inspired by the Rotta model we propose that the pressure-velocity interaction term appearing in (2.1) can be expressed as

$$-3\left(\overline{w'w'\frac{\partial p'}{\partial z}}\right) = \frac{3}{2}\frac{C_R}{\tau_s}\left(\frac{\overline{w'q}}{3} - \overline{w'w'^2}\right), \tag{2.4}$$

where τ_s is another decorrelation time that differs from τ. While expected to be small relative to the pressure-velocity interaction term, the viscous destruction contribution is herein retained and represented as (Zeman & Lumley 1976)

$$-2\nu\left(\overline{3w'\frac{\partial w'}{\partial x_i}\frac{\partial w'}{\partial x_i}}\right) = -2\overline{\epsilon' w'} = -c_2\frac{\overline{w'q}}{\tau_s}, \tag{2.5}$$

where c_2 is a similarity constant, and $\epsilon' \sim q/\tau_s$ is the fluctuating dissipation rate around $\bar{\epsilon}$. Inserting these approximations into (2.1) yields

$$\overline{w'^3} = -\frac{2}{3}\frac{(3 + 2a)\tau_s\sigma_w^2}{C_R}\frac{\partial \sigma_w^2}{\partial z} + \overline{w'q}\left(\frac{1}{3} - \frac{2c_2}{3C_R}\right). \tag{2.6}$$

A model for $\overline{w'q}$ is further needed to infer S_w. To arrive at this model, the K budget for the same flow conditions leading to (2.1) are employed. When mechanical production is

balanced by $\bar{\epsilon}$ as common in the ISL, the K budget leads to two outcomes (Lopez & García 1999):

$$u_*^2\frac{\partial \bar{u}}{\partial z} - \bar{\epsilon} = 0; \quad -\frac{1}{2}\frac{\partial \overline{w'q}}{\partial z} = 0. \tag{2.7a,b}$$

The height-independence of $\overline{w'q}$ is suggestive that it must be controlled by local conditions and a down-gradient approximation is justified given by (Lopez & García 1999)

$$-\frac{1}{2}\overline{w'q} = \kappa z u_* \frac{\partial K}{\partial z}. \tag{2.8}$$

The model in (2.8) has received experimental support even for rough-wall TBLs and across a wide range of Reynolds numbers and surface roughness values (Lopez & García 1999). Noting that $K \approx \sigma_u^2$ yields

$$\overline{w'^3} = -\frac{2}{3}\left[K_{t,w}\frac{\partial \sigma_w^2}{\partial z} + K_{t,u}\frac{\partial \sigma_u^2}{\partial z}\right]; \quad K_{t,w} = \frac{(3+2a)\tau_s\sigma_w^2}{C_R}; \quad K_{t,u} = \kappa z u_*\left(1 - \frac{2c_2}{C_R}\right), \tag{2.9a–c}$$

where $K_{t,w}$ and $K_{t,u}$ are eddy viscosity terms. These two eddy viscosity values become comparable in magnitude when setting $\tau_s = \kappa z/u_*$ (i.e. following classical ISL scaling) and $C_R = 1.8$ – its accepted value (Bou-Zeid *et al.* 2018) as expected in the ISL. To determine $\partial\sigma_w^2/\partial z$, the mean vertical-velocity equation is considered for the same idealized flow conditions as (2.1). This consideration results in

$$\frac{\partial \sigma_w^2}{\partial z} = -\left(\frac{1}{\rho}\right)\left(\frac{\partial \bar{P}}{\partial z}\right) - g, \tag{2.10}$$

where g is the gravitational acceleration. When $\bar{P} = -\rho g z$ (i.e. hydrostatic), $\partial\sigma_w^2/\partial z = 0$ or A_w is constant in z within the ISL. That is, the AEM requires $\bar{P}$ to be hydrostatic. However, the AEM precludes $\partial\sigma_u^2/\partial z = 0$ in the ISL. In fact, the AEM predicts $\partial\sigma_u^2/\partial z = -u_*^2 B_u/z$ when Re_τ is very large as expected in the ISL of an adiabatic atmosphere. Inserting this estimate into (2.9*a–c*), setting $u_* = \sigma_w/A_w$ and momentarily ignoring $\partial\sigma_w^2/\partial z$ relative to $\partial\sigma_u^2/\partial z$ as a simplification consistent with the AEM, leads to

$$S_w = \frac{\overline{w'^3}}{\sigma_w^3} = \frac{2}{3}\left(1 - \frac{2c_2}{C_R}\right)\frac{\kappa B_u}{A_w^3}. \tag{2.11}$$

This equation is the sought outcome. The term $2c_2/C_R$ reflects the relative importance of the pressure-velocity to viscous destruction terms. Pressure-velocity destruction effects are far more efficient than viscous effects supporting the argument that $2c_2/C_R \ll 1$ at very high Re_τ (Katul *et al.* 2013) such as the atmosphere. This implies that the numerical value of S_w, as obtained from (2.11), depends on three well-established phenomenological constants, namely κ, A_w and B_u (Banerjee & Katul 2013; Marusic & Monty 2019; Huang & Katul 2022), which, in turn, may depend weakly on Re_τ and the flow type. Equation (2.11) is also insensitive to the choices made for τ_s, because the AEM requires $\partial\sigma_w^2/\partial z = 0$.

3. Discussion and conclusion

From the $\overline{w'^3}$ local budget for a planar homogeneous and incompressible flow without subsidence, and upon assuming a (i) quasi-normal approximation for the fourth moment,

(ii) return-to-isotropy (or Rotta) model for pressure-velocity and viscous destruction, (iii) down-gradient approximation for the vertical TKE fluxes, and (iv) adopting the AEM for the second moments, a model (2.11) for S_w in the ISL was recovered. Equation (2.11) demonstrates two inter-related aspects about S_w in the ISL: (i) why S_w is positive and constant with z, and (ii) why conventional gradient-diffusion approximations fail to predict $\overline{w'^3}$ from $\partial\sigma_w^2/\partial z$.

Regarding the first, (2.11) predicts that $S_w > 0$ consistent with the paradigm that ejective eddy motions ($w' > 0, u' < 0$) are more significant in momentum transfer than sweeping motions ($w' < 0, u' > 0$) within the ISL. This assertion is supported by numerous experiments and simulations (Nakagawa & Nezu 1977; Raupach 1981; Heisel *et al.* 2020) and adds further confidence in the physics associated with the derivation of (2.11). Moreover, values of the constants in (2.11) for flat plate TBLs at $Re_\tau \to \infty$ correspond to $\kappa = 0.39$, $A_w = 1.33$ and $B_u = 1.26$ (Smits *et al.* 2011; Huang & Katul 2022). Upon further setting $c_2 = 0.1$ and $C_R = 1.8$ (conventional values) leads to $S_w = 0.12$. This estimate compares well with $S_w = 0.1$ reported for the ISL in the adiabatic atmosphere (Chiba 1978; Barskov *et al.* 2023) and, in general, with all the S_w data pertaining to very high Re_τ reported in figure 1 (i.e. ZM1–3 and PK). Note that for datasets pertaining to the low to moderate Re_τ (i.e. MN, DNS, HL1–2, PG1–3 and PR1–3), (2.11) cannot be used to estimate S_w using the AEM and the associated asymptotic values of A_w and B_u. However, figure 1 shows that these flows attain similar (i.e. slightly higher) and reasonably z-independent values of S_w. To explain this behaviour, it is necessary to step back to (2.9*a–c*). This formulation does not contain assumptions about the second moments (i.e. the AEM) and, once scaled with σ_w^3, represents a more general model for S_w. The only limitation is the need to provide reliable estimates of $\partial\sigma_w/\partial z$ and $\partial\sigma_u/\partial z$, which are here obtained from DNS data. Figure 2 indicates that, for most of the ISL, the first term on the right-hand side of (2.9*a*) is an order of magnitude smaller than the second and can be discarded as predicted by the AEM and advocated in the proposed theory. Predictions of S_w obtained from the second term are excellent in the ISL and resemble the observed z-independent behaviour. Besides providing further confidence on the proposed theory, this result indicates that, since $K_{t,u}$ is directly proportional to z, $\partial\sigma_u^2/\partial z$ must overall scale as $\sim 1/z$, as predicted by the AEM. Hence, we argue that the AEM represents a reasonable approximation provided B_u and A_w are adjusted to accommodate for low Re_τ effects. As shown in figure 3, this is the case for DNS and all laboratory data.

For the DNS, appropriate values of $A_w(= 1.15\text{–}1.17)$ and $B_u(= 0.85\text{–}0.86)$ were estimated by fitting the AEM to the available data for all available Re_τ. The constant $\kappa = 0.39$ was assumed as reported in the literature (Marusic *et al.* 2013; Peruzzi *et al.* 2020). When inserting these choices of A_w and B_u from the DNS into (2.11), the computed $S_w = 0.13$, which is close to reported values in figure 1(*c*). The same approach was used for all laboratory studies. When combining all the runs together (wind tunnel, pipe flow and open channel flow), ensemble-averaged $A_w = 1.04 \pm 0.12$ and the ensemble-averaged $B_u = 0.78 \pm 0.23$ were obtained across runs within an experiment and across experiments. These values result in an ensemble-averaged $S_w = 0.17 \pm 0.07$ and agree with the measurements reported in figure 1.

This analysis and figure 1 suggest that S_w for DNS and experiments is higher than 0.12 estimated for $Re_\tau \to \infty$. This is probably because of deviations of B_u and A_w from their asymptotic values. The effects of such deviations on S_w are, however, modest because, although values of A_w and B_u are significantly lower than their counterparts at $Re_\tau \to \infty$ (i.e. $A_w = 1.33$ and $B_u = 1.26$, see table 1), (2.11) indicates that S_w is dictated by B_u/A_w^3, meaning the effect of such deviations are in good part compensated.

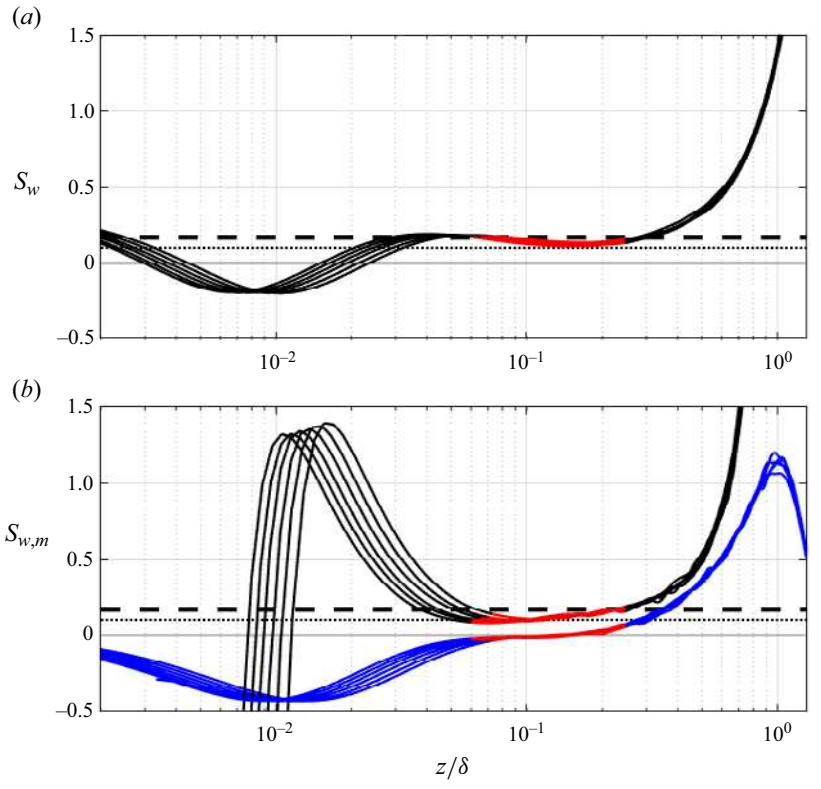

Figure 2. (*a*) Variation of the vertical-velocity skewness S_w with normalized wall-normal distance z/δ from DNS Sillero *et al.* (2013); (*b*) $S_{w,m}$ is the modelled skewness using the first term (blue line) and second term (black line) on the right-hand side of (2.9*a–c*) both scaled with σ_w^3. In both panels, red lines identify the ISL range. The dashed line is $S_w = 0.16$ and the dotted line is $S_w = 0.10$.

Additionally, a separate investigation into the vertical extent of the constant S_w region was conducted using laboratory data. This was achieved by selecting data points varying within a 5 % range around the S_w mode. The analysis revealed that the constant S_w region extends from $1.13–2.51\sqrt{Re_\tau}\nu/u_*$ to $0.16–0.32\delta$, which is very similar to the range that is commonly employed to identify the ISL using other velocity statistics (i.e. from $2.6\sqrt{Re_\tau}\nu/u_*$ to $0.15 - 0.25\delta$) (Zhou & Klewicki 2015; Örlü *et al.* 2016, 2017). This analysis provides further evidence of the operational interlink between the constant S_w region and the ISL.

Regarding the second feature of (2.11), (2.9*a–c*) offers an explanation as to why conventional down-gradient closure models with eddy viscosity $K_t \propto \bar{q} l_m$ (l_m is a 'master' mixing length) expressed in general index notation ($[u_1', u_2', u_3'] = [u', v', w']$) as (Launder, Reece & Rodi 1975)

$$\overline{u_i' u_j' u_k'} = -K_t \left[\frac{\partial \overline{u_i' u_j'}}{\partial x_k} + \frac{\partial \overline{u_i' u_k'}}{\partial x_j} + \frac{\partial \overline{u_j' u_k'}}{\partial x_i} \right] \tag{3.1}$$

spectacularly fail when $i = j = k = 3$ and when A_w is approximately constant in the ISL as in the AEM. Yet, the derived equation here also offers a rectification based on the AEM. This rectification accommodates the role of finite $\partial \sigma_u^2/\partial z$ on $\overline{w'^3}$ that cannot arise from (3.1). In conclusion, this paper demonstrates that, within the ISL of turbulent and adiabatic

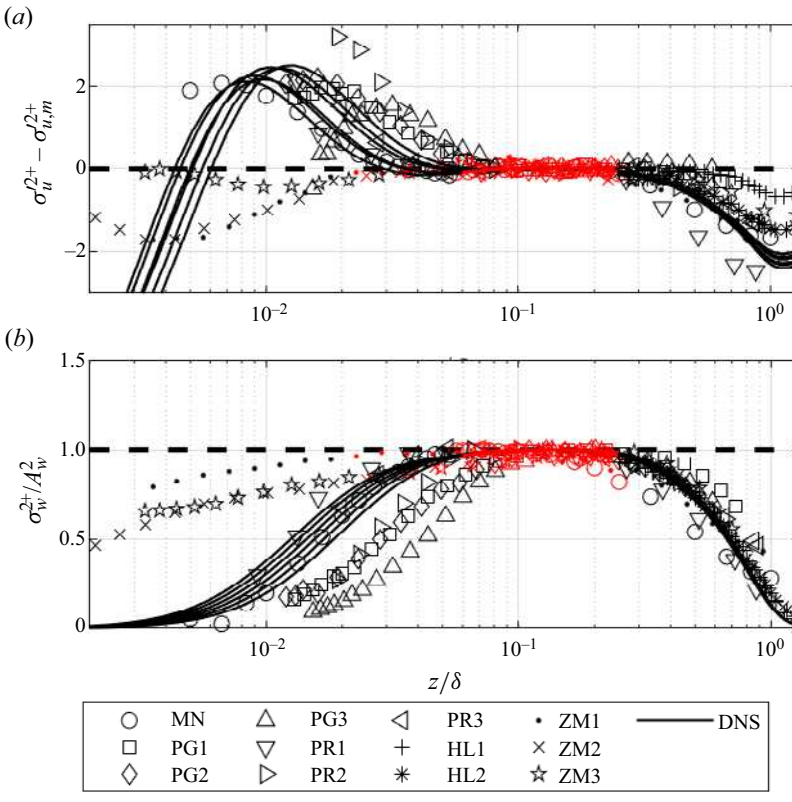

Figure 3. (*a*) Difference between σ_u^{2+} and estimations obtained from the AEM, $\sigma_{u,m}^{2+} = A_u - B_u \log(z/\delta)$ using values of A_u and B_u obtained from regression of data within the ISL range (identified by red symbols and lines) vs wall-normal distance z/δ; (*b*) non-dimensional vertical-velocity variance σ_w^2 normalized with A_w obtained from data fitting within the ISL (identified by red symbols and lines) vs wall-normal distance z/δ. Data sources and references are summarized in table 1.

smooth-wall flows, S_w attains z-independent values that are predictable from well-known turbulence constants relating to the AEM. This behaviour is reported for a variety of different wall flows and is fairly independent of variations in Re_τ, hence universal and robust.

Supplementary material. The data that support the findings of this study are available from the corresponding author upon reasonable request.

Acknowledgements. The authors thank J.C. Klewicki for providing the ZM and PK datasets.

Funding. E.B. acknowledges the support from Politecnico di Torino for visiting Duke University. G.K. acknowledges support from the U.S. National Science Foundation (NSF-AGS-2028633) and the U.S. Department of Energy (DE-SC0022072). D.V. and C.M. acknowledge the European Union's Horizon 2020 research and innovation programme under the Marie Sklodowska-Curie grant agreement no. 101022685 (SHIEELD). D.P. acknowledges support from Fondo europeo di sviluppo regionale (FESR) for project Bacini Ecologicamente sostenibili e sicuri, concepiti per l'adattamento ai Cambiamenti ClimAtici (BECCA) in the context of Alpi Latine COoperazione TRAnsfrontaliera (ALCOTRA) and project Nord Ovest Digitale e Sostenibile – Digital innovation toward sustainable mountain (Nodes – 4).

Declaration of interests. The authors report no conflict of interest.

Author ORCIDs.
Elia Buono https://orcid.org/0009-0009-6666-1753;
Gabriel Katul https://orcid.org/0000-0001-9768-3693;
Michael Heisel https://orcid.org/0000-0002-4200-5550;
Davide Vettori https://orcid.org/0000-0001-5121-4197;
Davide Poggi https://orcid.org/0000-0003-0024-3574;
Cosimo Peruzzi https://orcid.org/0000-0002-1418-9575;
Costantino Manes https://orcid.org/0000-0002-3990-7449.

References

André, J.C., De Moor, G., Lacarrere, P. & Du Vachat, R. 1976 Turbulence approximation for inhomogeneous flows. Part I. The clipping approximation. *J. Atmos. Sci.* **33** (3), 476–481.

Bærentsen, J. & Berkowicz, R. 1984 Monte Carlo simulation of plume dispersion in the convective boundary layer. *Atmos. Environ.* **18** (4), 701–712.

Banerjee, T. & Katul, G.G. 2013 Logarithmic scaling in the longitudinal velocity variance explained by a spectral budget. *Phys. Fluids* **25** (12), 125106.

Barskov, K., Chechin, D., Drozd, I., Artamonov, A., Pashkin, A., Gavrikov, A., Varentsov, M., Stepanenko, V. & Repina, I. 2023 Relationships between second and third moments in the surface layer under different stratification over grassland and urban landscapes. *Boundary-Layer Meteorol.* **187** (1), 311–338.

Bogenschutz, P.A., Gettelman, A., Morrison, H., Larson, V.E., Schanen, D.P., Meyer, N.R. & Craig, C. 2012 Unified parameterization of the planetary boundary layer and shallow convection with a higher-order turbulence closure in the Community Atmosphere Model: single-column experiments. *Geosci. Model Dev.* **5** (6), 1407–1423.

Bou-Zeid, E., Gao, X., Ansorge, C. & Katul, G.G. 2018 On the role of return to isotropy in wall-bounded turbulent flows with buoyancy. *J. Fluid Mech.* **856**, 61–78.

Canuto, V.M., Minotti, F., Ronchi, C., Ypma, R.M. & Zeman, O. 1994 Second-order closure PBL model with new third-order moments: comparison with LES data. *J. Atmos. Sci.* **51** (12), 1605–1618.

Chiba, O. 1978 Stability dependence of the vertical wind velocity skewness in the atmospheric surface layer. *J. Meteorol. Soc. Japan. Ser.* II **56** (2), 140–142.

Flack, K.A., Schultz, M.P. & Connelly, J.S. 2007 Examination of a critical roughness height for outer layer similarity. *Phys. Fluids* **19** (9), 095104.

Heisel, M., Katul, G.G., Chamecki, M. & Guala, M. 2020 Velocity asymmetry and turbulent transport closure in smooth-and rough-wall boundary layers. *Phys. Rev. Fluids* **5** (10), 104605.

Huang, K.Y. & Katul, G.G. 2022 Profiles of high-order moments of longitudinal velocity explained by the random sweeping decorrelation hypothesis. *Phys. Rev. Fluids* **7** (4), 044603.

Huang, M., Xiao, H., Wang, M. & Fast, J.D. 2020 Assessing CLUBB PDF closure assumptions for a continental shallow-to-deep convective transition case over multiple spatial scales. *J. Adv. Model. Earth Syst.* **12** (10), e2020MS002145.

Katul, G.G., Porporato, A., Manes, C. & Meneveau, C. 2013 Co-spectrum and mean velocity in turbulent boundary layers. *Phys. Fluids* **25** (9), 091702.

Launder, B.E., Reece, G. & Rodi, W. 1975 Progress in the development of a Reynolds-stress turbulence closure. *J. Fluid Mech.* **68** (3), 537–566.

Li, T., Wang, M., Guo, Z., Yang, B., Xu, Y., Han, X. & Sun, J. 2022 An updated CLUBB PDF closure scheme to improve low cloud simulation in CAM6. *J. Adv. Model. Earth Syst.* **14** (12), e2022MS003127.

Lopez, F. & García, M.H. 1999 Wall similarity in turbulent open-channel flow. *J. Engng Mech.* **125** (7), 789–796.

Luhar, A.K. & Britter, R.E. 1989 A random walk model for dispersion in inhomogeneous turbulence in a convective boundary layer. *Atmos. Environ.* **23** (9), 1911–1924.

Manes, C., Poggi, D. & Ridolfi, L. 2011 Turbulent boundary layers over permeable walls: scaling and near-wall structure. *J. Fluid Mech.* **687**, 141–170.

Marusic, I. & Monty, J.P. 2019 Attached eddy model of wall turbulence. *Annu. Rev. Fluid Mech.* **51**, 49–74.

Marusic, I., Monty, J.P., Hultmark, M. & Smits, A.J. 2013 On the logarithmic region in wall turbulence. *J. Fluid Mech.* **716**, R3.

MAURIZI, A. & TAMPIERI, F. 1999 Velocity probability density functions in Lagrangian dispersion models for inhomogeneous turbulence. *Atmos. Environ.* **33** (2), 281–289.

MELLOR, G. & YAMADA, T. 1982 Development of a turbulence closure model for geophysical fluid problems. *Rev. Geophys.* **20** (4), 851–875.

MENEVEAU, C. 1991 Analysis of turbulence in the orthonormal wavelet representation. *J. Fluid Mech.* **232**, 469–520.

MENEVEAU, C. & MARUSIC, I. 2013 Generalized logarithmic law for high-order moments in turbulent boundary layers. *J. Fluid Mech.* **719**, R1.

MORRILL-WINTER, C., KLEWICKI, J., BAIDYA, R. & MARUSIC, I. 2015 Temporally optimized spanwise vorticity sensor measurements in turbulent boundary layers. *Exp. Fluids* **56** (12), 216.

NAKAGAWA, H. & NEZU, I. 1977 Prediction of the contributions to the Reynolds stress from bursting events in open-channel flows. *J. Fluid Mech.* **80** (1), 99–128.

ÖRLÜ, R., FIORINI, T., SEGALINI, A., BELLANI, G., TALAMELLI, A. & ALFREDSSON, P.H. 2017 Reynolds stress scaling in pipe flow turbulence—first results from CICLoPE. *Phil. Trans. R. Soc.* A **375** (2089), 20160187.

ÖRLÜ, R., SEGALINI, A., KLEWICKI, J. & ALFREDSSON, P.H. 2016 High-order generalisation of the diagnostic scaling for turbulent boundary layers. *J. Turbul.* **17** (7), 664–677.

PERUZZI, C., POGGI, D., RIDOLFI, L. & MANES, C. 2020 On the scaling of large-scale structures in smooth-bed turbulent open-channel flows. *J. Fluid Mech.* **889**, A1.

POGGI, D., PORPORATO, A. & RIDOLFI, L. 2002 An experimental contribution to near-wall measurements by means of a special laser Doppler anemometry technique. *Exp. Fluids* **32** (3), 366–375.

PRIYADARSHANA, P.J.A. & KLEWICKI, J.C. 2004 Study of the motions contributing to the Reynolds stress in high and low Reynolds number turbulent boundary layers. *Phys. Fluids* **16** (12), 4586–4600.

RAUPACH, M.R. 1981 Conditional statistics of Reynolds stress in rough-wall and smooth-wall turbulent boundary layers. *J. Fluid Mech.* **108**, 363–382.

ROTTA, J. 1951 Statistische Theorie nichthomogener Turbulenz. *Z. Phys.* **129** (6), 547–572.

SCHULTZ, M.P. & FLACK, K.A. 2007 The rough-wall turbulent boundary layer from the hydraulically smooth to the fully rough regime. *J. Fluid Mech.* **580**, 381–405.

SILLERO, J.A., JIMÉNEZ, J. & MOSER, R.D. 2013 One-point statistics for turbulent wall-bounded flows at Reynolds numbers up to $\delta+ = 2000$. *Phys. Fluids* **25** (10), 105102.

SMITS, A.J., MCKEON, B.J. & MARUSIC, I. 2011 High-Reynolds number wall turbulence. *Annu. Rev. Fluid Mech.* **43** (1), 353–375.

STEVENS, R., WILCZEK, M. & MENEVEAU, C. 2014 Large-eddy simulation study of the logarithmic law for second-and higher-order moments in turbulent wall-bounded flow. *J. Fluid Mech.* **757**, 888–907.

TOWNSEND, A.A.R. 1976 *The Structure of Turbulent Shear Flow*. Cambridge University Press.

WOODCOCK, J.D. & MARUSIC, I. 2015 The statistical behaviour of attached eddies. *Phys. Fluids* **27** (1), 015104.

WYNGAARD, J.C. 2010 *Turbulence in the Atmosphere*. Cambridge University Press.

WYNGAARD, J.C. & WEIL, J.C. 1991 Transport asymmetry in skewed turbulence. *Phys. Fluids* A **3** (1), 155–162.

ZEMAN, O. & LUMLEY, J.L. 1976 Modeling buoyancy driven mixed layers. *J. Atmos. Sci.* **33** (10), 1974–1988.

ZHAO, R. & SMITS, A.J. 2007 Scaling of the wall-normal turbulence component in high-Reynolds-number pipe flow. *J. Fluid Mech.* **576**, 457–473.

ZHOU, A. & KLEWICKI, J. 2015 Properties of the streamwise velocity fluctuations in the inertial layer of turbulent boundary layers and their connection to self-similar mean dynamics. *Intl J. Heat Fluid Flow* **51**, 372–382.

ZIMMERMAN, S. 2019 Experimental investigation of velocity and vorticity in turbulent wall flows. PhD thesis, The University of Melbourne, Australia.